ACS OMEGA

http://pubs.acs.org/journal/acsodf

Article

Microscopic Proof of Photoluminescence from Mechanochemically Synthesized 1-Octene-Capped Quantum-Confined Silicon Nanoparticles: Implications for Light-Emission Applications

Ankit Goyal,* Marco van der Laan, Alessandro Troglia, Min Lin, Harshal Agarwal, Jorik van de Groep, Roland Bliem, Jos M. J. Paulusse, Peter Schall, and Katerina Dohnalova

Cite This: *ACS Omega* 2022, 7, 24881−24887

Read Online

ACCESS | Metrics & More | Article Recommendations | Supporting Information

Downloaded via AMOLF on August 12, 2022 at 12:56:25 (UTC).
See https://pubs.acs.org/sharingguidelines for options on how to legitimately share published articles.

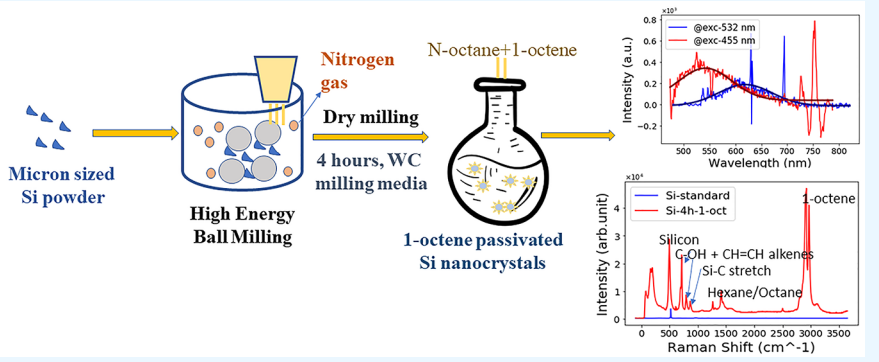

ABSTRACT: Silicon nanoparticles (SiNPs) have been explored intensively for their use in applications requiring efficient fluorescence for LEDs, lasers, displays, photovoltaic spectral-shifting filters, and biomedical applications. High radiative rates are essential for such applications, and theoretically these could be achieved via quantum confinement and/or straining. Wet-chemical methods used to synthesize SiNPs are under scrutiny because of reported contamination by fluorescent carbon species. To develop a cleaner method, we utilize a specially designed attritor type high-energy ball-mill and use a high-purity (99.999%) Si microparticle precursor. The mechanochemical process is used under a continuous nitrogen gas atmosphere to avoid oxidation of the particles. We confirm the presence of quantum-confined NPs (<5 nm) using atomic force microscopy (AFM). Microphotoluminescence (PL) spectroscopy coupled to AFM confirms quantum-confined tunable red/near-infrared PL emission in SiNPs capped with an organic ligand (1-octene). Using micro-Raman-PL spectroscopy, we confirm SiNPs as the origin of the emission. These results demonstrate a facile and potentially scalable mechanochemical method of synthesis for contamination-free SiNPs.

1. INTRODUCTION

Silicon is a nontoxic, earth-abundant semiconductor with a bulk indirect band gap of 1.12 eV.[1,2] It is a suitable material for photovoltaic (PV) applications and currently has the lion's share in the PV market.[3] Its indirect band gap and low quantum yield, however, make it unsuitable for applications requiring efficient fluorescence, such as LEDs, lasers, displays, and biomedical applications. Theoretical studies suggest the possibility of quasi-direct band gap formation with radiative rates comparable to those of direct band gap materials in quantum-confined silicon with an organic coating and/or heavily strained SiNPs.[4−8] Over the past few decades, several reports have claimed the synthesis of quantum-confined SiNPs of size <5 nm (Bohr radius) with observable visible light photoluminescence (PL).[9−14] Synthesis processes such as wet-chemical synthesis, plasma synthesis, and electrochemical etching were used to synthesize hydrogen-capped, oxide-capped, and organically capped SiNPs with spectrally tunable fluorescence throughout the visible part of the spectrum.[9−15] The common challenge with all of these reported methods is their limited scalability, which makes the quantum dots unsuitable for industrial applications. Hydrogen-capped SiNPs are unstable in air because they are prone to oxidation and impurity-related red PL with a slow radiative rate.[1] From this type of SiNPs blue PL with a fast radiative rate[1] has also been reported, but it has an unclear origin.[16] SiNPs with sizes near the excitonic Bohr radius (∼5 nm) show size-tunable PL in the near-infrared (IR) range.[17,18] Alkyl-ligand-passivated SiNPs are the most stable against oxidation and have reported

Received: May 31, 2022
Accepted: June 22, 2022
Published: July 8, 2022

© 2022 The Authors. Published by American Chemical Society

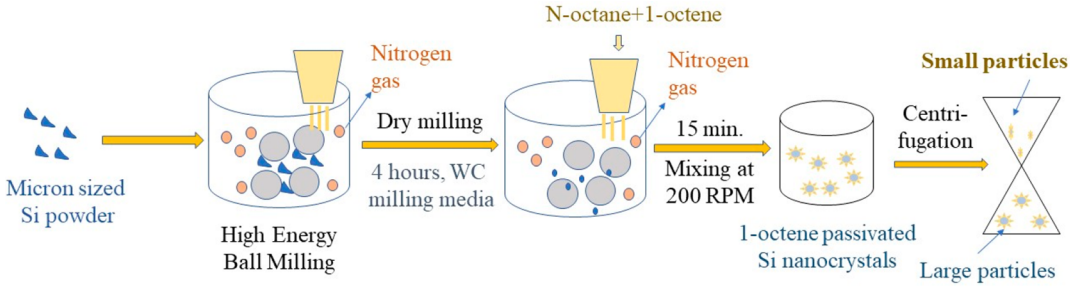

Figure 1. High-energy mechanochemical synthesis scheme of 1-octene-capped SiNPs.

tunability throughout the entire visible range.[7,19−22] Such SiNPs are typically synthesized by wet-chemical methods that involve higher temperatures in the presence of carbon sources during the synthesis process that has been recently reported to lead to the cosynthesis of various carbon-related fluorescent material, such as carbon dots[23−25] along with the SiNPs in the sample. Recent critical reports have also shown that even without Si precursors, the product still has optical properties similar to those reported for SiNPs,[26−28] which strengthens the argument of contamination by brightly fluorescent carbon species causing the reported bright PL, instead of silicon.

Thus, several challenges remain: (1) a synthesis method that could produce large quantities of SiNPs without contamination; (2) direct and unambiguous proof of PL emission from SiNPs; and (3) visible-light-tunable PL corroborating the theoretical studies.[29,30] One way to overcome the issue of carbon contamination and up-scalability is to use a top-down solvent-free approach, starting with pure silicon. Regarding this, in 2007, Heintz et al. first reported the synthesis of luminescent silicon nanoparticles (SiNPs) by high-energy ball-milling.[31] Millimeter-sized silicon particles were crushed in a mill in the presence of alkenes and alkynes for surface passivation, and blue PL emission was observed. This study shows the potential of mechanochemistry in the synthesis of SiNPs, although the authors observed the debated fast-decaying blue PL and no proof related to carbon contamination of the free SiNPs was provided. Later, Matsumoto et al. observed PL in the blue spectral range from milled SiNPs originating from dimethylanthracene (DMA) impurities in hexane.[28] In our recent study, we also observed blue PL from high-energy ball-milled SiNPs capped with oxides, likely originating from metallic defects introduced into the SiNPs during the ball-milling from the milling media (balls and vessel).[32] These experiments highlight the importance of experimental scrutiny to minimize the contamination and assumptions.

Here, we report the synthesis of very pure 1-octene (alkene)-capped SiNPs by high-energy ball-milling. A custom-built high-energy ball-mill is used in the process to avoid any exposure of oxygen during the process. The insertion of organic ligands was done near the end of the process to avoid the formation of carbon dots during the milling process, which involves high pressures and heat. Tungsten carbide (WC) is used as a milling medium to prevent metallic impurities from inserting into the SiNPs. WC is a harder material than silicon, so the diffusion of WC in silicon is unlikely. We use dry milling to avoid any contamination from the organic solvents. Size-dependent PL is studied using AFM correlated with micro-PL spectroscopy, matching the theory proposed by Wang et al. and Delerue et al.[29,30] We confirm the origin of the PL to be from 1-octene -capped SiNPs by microscopic Raman-PL correlated spectroscopy. The results of this work offer an unambiguous demonstration of the origin of PL from SiNPs and the potential of mechanochemistry for the synthesis of SiNPs.

2. MATERIALS AND METHODS

Crystalline silicon powder of 20 μm size and 99.999% purity was purchased from Hongwu International Group Ltd., China. The full process scheme is depicted in Figure 1. We followed the synthesis process as described in our previous reports with a difference in the addition of ligands at the end of the milling process.[32,33] Silicon powder (1 g) is loaded into a custom-built attritor-type high-energy ball-mill vessel. A WC milling medium is used in the process. The Si powder is ball-milled at 450 rpm at a ball-to-powder weight ratio of 40:1 for 4 h. Milling is performed in steps of 1 h of milling followed by 15 min of cooling, assisted by continuous water circulation around the milling vessel through a jacket to remove excess heat generated during the milling process. Continuous nitrogen gas flow is provided to avoid atmospheric oxygen reacting with the silicon powder during the milling process. After the milling process is finished, a syringe is used to insert 1-octene (ligand) and octane as a solvent through a gas inlet nozzle without opening the milling vessel. The colloidal dispersion of 1-octene-passivated SiNPs in octane is then collected.

The SiNP dispersion is centrifuged at 12 000 rpm for 10 min to collect the precipitate. The supernatant is discarded because it contains unreacted ligands and excess solvent. The precipitate is redispersed in octane. The precipitate is rinsed with octane three times by a centrifugation−sonication cycle. The cleaned colloidal dispersion was left to rest overnight to allow the larger particles to sediment at the bottom. The supernatant is collected and then centrifuged again to get the size-separated colloidal dispersion of SiNPs in octane. The collected colloidal dispersion is stored in a glass vial sealed with Teflon tape.

A Bruker Alpha Fourier-transform infrared spectroscopy (FTIR) spectrometer equipped with an attenuated total reflection (ATR) single-reflection crystal (Bruker Optic GmbH, Ettlingen, Germany) is used to record FTIR spectra of unmilled and milled Si powder samples. Dynamic light scattering (DLS) of milled Si samples was measured with a Zetasizer Nano ZS (633 nm, scattering angle 173°, Malvern Instruments, Herrenberg, Germany). For single-nanoparticle PL spectroscopy, SiNPs were dispersed in spectroscopy-grade hexane and drop-cast on a quartz coverslip (SPI supplies 25-mm-diameter coverslipw with a thickness of 0.15−0.18 mm) and left to dry in air at room temperature. For the measurement, we use a Zeiss optical microscope (inverted,

https://doi.org/10.1021/acsomega.2c03396
ACS Omega 2022, 7, 24881−24887

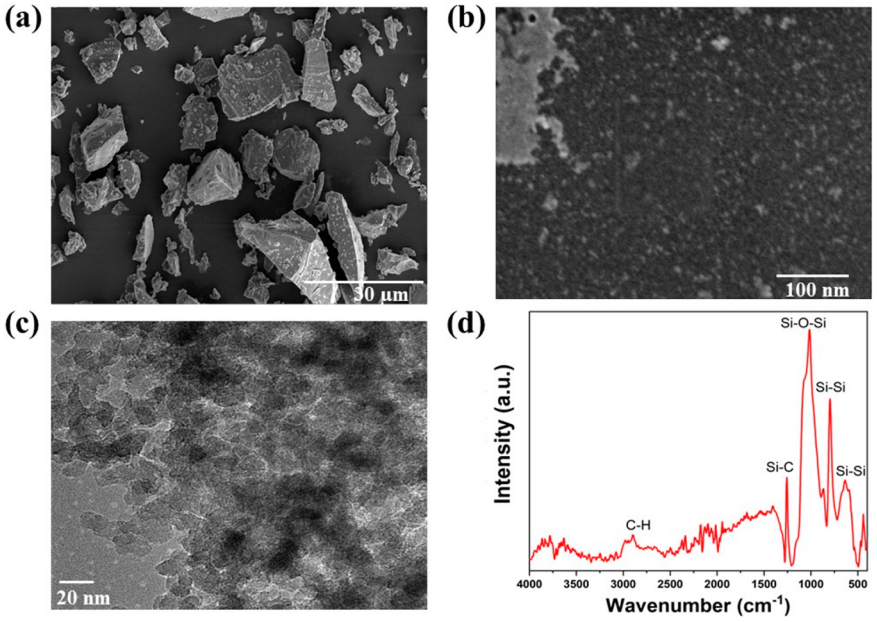

Figure 2. (a) SEM image of the micrometer-sized silicon particles before milling. (b) SEM image of size-separated SiNPs after milling. (c) TEM image of size-separated SiNPs. (d) FTIR spectrum of milled SiNPs.

Axio Observer 3) coupled to an atomic force microscope (AFM; Nanowizard 3, JPK Instruments). The PL emission is measured using a spectrometer (Princeton Instruments, Acton SP2300) with a charge-coupled detector (CCD; Princeton Instruments, Pylon 400B), coupled to the optical microscope. A diode laser (445 nm, Becker and Hickl GmbH, BDL-445-SMN) is used to excite the samples. The PL from the sample is collected using a 100× objective (Zeiss, Epiplan-Neofluar with NA = 0.75) and is spectrally filtered using a razor-edge 445 nm band-pass filter (Semrock, BLP01−445R-25) to remove the scattered excitation light. Correlated Raman and PL spectroscopy measurements are employed to correlate the particle composition and PL. For this purpose, SiNPs dispersed in octane are drop cast on a saphhire substrate and left to dry in air at room temperature. Measurements are performed on a Witec alpha300R confocal microscope excited by a diode-pumped solid-state 532 nm laser. Alternatively, samples are excited by 455 nm laser light, generated by a NKT Photonics SuperK Extreme white-light supercontinuum laser with a wavelength range of 450−2200 nm, coupled to an NKT Photonics SuperK Select acousto-optical tunable filter for wavelength selection. The excitation light is directed onto the sample via a 100× objective with NA = 0.9 (Zeiss EC Epiplan-Neofluar 100x) which also out-coupled the resultant Raman and PL signals into a spectrograph (Witec UHTS 300 VIS) and detected with a CCD (Ador EMCCD). Raman and PL spectra are measured using 1800 and 150 gr/mm gratings, respectively.

X-ray diffraction (XRD) studies are performed using a Rigaku Miniflex II Desktop X-ray diffractometer with Cu Kα radiation (λ = 1.5406 Å). Scanning electron microscopy (SEM) measurements are performed using a Verios 460 STEM. An energy-dispersive spectroscopy (EDX) Oxford Xmax 80 mm^2 silicon drift detector is attached to a STEM setup to study elemental composition. Transmission electron microscopy (TEM) is performed using the Technai G2 20 X-Twin equipped with a field emission gun (FEG) as the electron source. X-ray photoelectron spectroscopy (XPS) is performed in an ultrahigh vacuum setup (base pressure better than 1.0 × 10^{-9} mbar) equipped with a Scienta Omicron R4000 HiPP-3 hemispherical analyzer (swift acceleration mode, 1 mm slit entrance) and a monochromated Al Kα X-ray source (1486.6 eV). The samples are mounted on standard Omicron flagpoles with double-sided Cu tape. The spectra are acquired at 100 eV of pass energy (PE) and calibrated to the peak position of O 1s in SiO_2 (532.9 eV binding energy).

3. RESULTS AND DISCUSSION

We start our analysis by characterizing the particle size of the silicon powder before and after the milling process using SEM, where images of unmilled particles indicate the presence of micrometer-sized particles, (Figure 2a) which are downsized to SiNPs by the high-energy ball-milling process (Figure 2b). The SEM images clearly show the presence of nanosized Si particles in the milled Si sample. The presence of SiNPs with sizes below 20 nm is further confirmed by TEM measurements (Figure 2c). Next, we assess the capping and surface termination by FTIR (Figure 2d), which show evidence of organically capped Si particles in the milled sample, noted by the presence of peaks at 1257 and 806 cm^{-1} corresponding to Si−C and Si−Si bonds, suggesting the formation of organic bonds on the surface of the SiNPs.[31] However, the sample also reveals Si−O bonds, suggesting that the sample is not completely capped with 1-octene and may have a mixture of 1-octene and oxygen-capped SiNPs. This has also been reported in similar synthesis methods.[25] It could be caused by the fact that the starting Si microparticles are oxide-capped, which might also persist in the final product. The presence of oxygen in the silicon particles before and after milling is confirmed by the XPS measurements (Figure S1).

In addition to SEM, TEM, and FTIR analysis, we employ a series of additional characterization methods to analyze the sample. XRD demonstrates that the milling process does not change the phase of the particles (Figure S2). DLS is used to characterize the particle size distribution, indicating a

https://doi.org/10.1021/acsomega.2c03396
ACS Omega 2022, 7, 24881−24887

reduction of particle sizes from ∼20 to 0.1−1 μm after milling (Figure S3).

EDX analysis (Figure S4) shows the presence of silicon, carbon, and oxygen in the sample, which is expected, considering the composition of the starting material (pure silicon) and the use of carbon ligands. Oxygen was present in trace amounts in the starting material. The absence of other elements suggests negligible contamination in the milled samples.

The main challenge lies in the unambiguous identification of the PL emission source. In particular, the PL emission originates from the SiNPs and not some carbon-related fluorescent material and is proof of its tuneability by the nanoparticle's size rather than being impurity-related. We solve these challenges using two correlated measurements: (1) microscopic PL spectroscopy correlated with size measured by coupled AFM and (2) microscopic Raman spectroscopy correlated with PL measurements.

After the size-separation process described in the Materials and Methods section, we could identify a fraction of nanosized (<10 nm) particles in the sample (Figure 2b). A diluted dispersion of SiNPs is then drop cast on a transparent quartz substrate (∼150 μm thickness). We perform AFM to measure particle sizes in the size-separated milled sample (Figure S5). A histogram obtained from AFM is shown in the inset of Figure S5, suggesting particle sizes ranging from 2 to 6 nm with an approximated average size of ∼4.2 nm, well within the onset of the regime of quantum confinement in silicon. The SiNPs show size-dependent PL emission, an expected result from quantum confinement. We measure PL from single SiNPs using our optical microspectroscopy setup, and the size of the emitting particles is directly measured using a coupled AFM. First, we record a PL image in wide-field imaging mode (Figure 3a) with an acquisition time of 10 s to avoid photobleaching of the SiNPs. The PL image shows agglomerated NPs, similar to what we observed in TEM and SEM images (Figure 2b,c). This agglomeration restricts us from correlating the single-dot PL with its AFM profile directly, as we have done in the past on a different material.[34] The same area of the PL image is subsequently slowly scanned with AFM in tapping mode (part of the scanned region is shown in Figure 3b) to measure the size of SiNPs and to confirm whether the SiNPs are agglomerated, which is indeed observed. We could find a pattern in the clustered NPs by observing real-time AFM tip movement on the image constructed by CCD, and that is highlighted by a red square. The sizes of these clusters are still <7 nm. However, there are several NPs observed in between the large clusters that might be isolated and exhibit size-correlated PL emission. The single particles and the clusters of particles are shown by black and white arrows, respectively, in Figure 3b. Because the emission from the NPs is very weak and somewhat overshadowed by the clusters present in their vicinity, we measured the PL spectrum using a narrow vertical slit (2 × 80 μm^2) and scanned the sample in steps of ∼2 μm using the motorized AFM stage controller. The measured PL spectrum of the NPs shows PL varying from 550 to 700 nm, as shown in Figure 3c. The PL peak positions correlate well with particle size as expected from the literature[29,30,35] and thus suggest size-dependent emission.

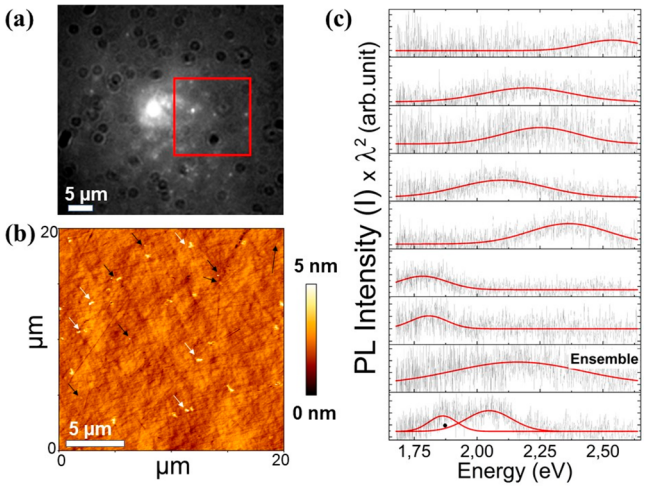

Figure 3. (a) 2D PL micrograph of emitting SiNPs. The red square indicates the region corresponding to the AFM scan in the figure below. (b) Corresponding AFM scan of a similar area showing agglomerated SiNPs. Black and white arrows are used to show the single nanoparticles and clusters of particles, respectively. (c) Gaussian peak fitting of the measured PL spectrum shows PL emission ranging from 550 to 700 nm.

In view of these results, we now revisit the discussion on potential PL emission from carbon-related species as an alternative interpretation. It is thus very important to verify that the PL emitting particles are 1-octene-capped SiNPs and not some carbon (or other) contamination. This is confirmed by micro-Raman-PL spectroscopy on a Witec microscope. Acquired dark-field images of milled SiNPs are shown in Figure 4a. The imaging is based on scattering; bright spots are due to agglomerates causing increased scattering, whereas the overall scale is unrelated to the size of the nanoparticles. From the particles visible in the optical image, a few were randomly selected for correlative PL and Raman analysis. Figure 4b,c shows Raman spectra of the sample (solid red curve) and a reference standard silicon wafer (solid blue curve) obtained by illuminating the sample with a 532 nm laser. The milled silicon particles show a 495 cm^{-1} Raman shift compared to bulk silicon's 520 cm^{-1} shift,[36] which indeed suggests the presence of SiNPs. Because there is no Raman peak at 480 cm^{-1} (Figure 4c), this confirms the absence of amorphous silicon particles,[37] concomitant with the XRD results. Furthermore, vibrations of 1-octene, Si−C, and alkane bonds are observed, as shown in Figure 4b, suggesting the successful passivation of the SiNPs[38−40] and/or the possible presence of the SiC material, indicated by the XRD measurements. Subsequently, after the micro-Raman spectroscopy measurement we also measured PL emission (on the same SiNPs) to correlate the micro-Raman results with the PL spectra (Figure 4d). Indeed, the measured PL spectra are consistent with the emission characteristics of SiNPs.[29,30,35] To fully establish this link, we use the excitation wavelengths of 455 nm in addition to the 532 nm excitation, which we can directly compare with the results of Figure 3c. The recorded spectrum lies in the range of the single-particle spectra peaking between 1.8 and 2.5 eV and is close to the measured ensemble spectrum (Figure 3c).

A correlated measurement of an SiNP-like PL spectrum (Figure 4d) (that closely resembles the ensemble PL spectrum) from the same particle that exhibits a Raman spectrum expected for 1-octene-capped SiNPs (Figure 4b) confirms that the PL does indeed originate from 1-octene-capped SiNPs. It also shows the important role and potential of the correlative micro-Raman-PL spectroscopy technique in the

https://doi.org/10.1021/acsomega.2c03396
ACS Omega 2022, 7, 24881−24887

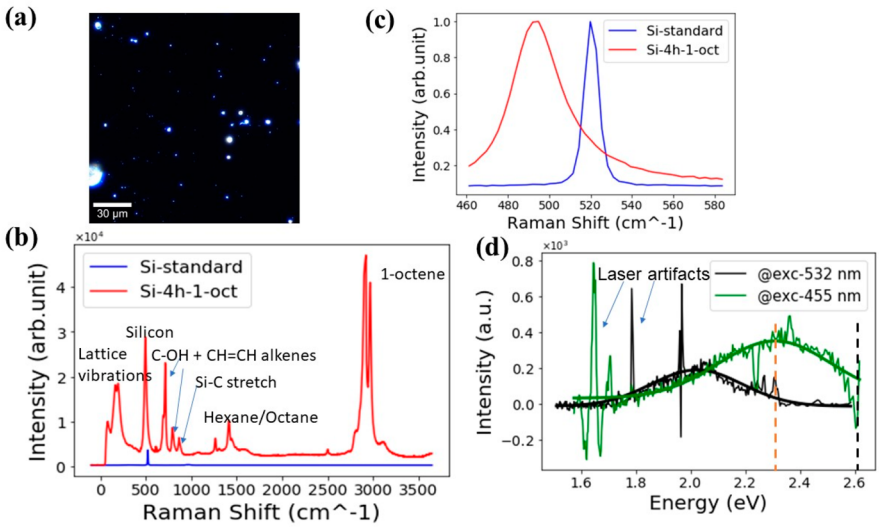

Figure 4. Micro-Raman-correlated PL spectroscopy of the 1-octene-capped SiNPs. (a) Dark-field optical image of the SiNPs drop cast on a sapphire substrate. (b) Micro-Raman spectrum of the SiNPs (in red), showing the presence of vibrations related to the nanocrystalline silicon and organic ligands. The bulk Si Raman spectrum is shown (in blue) for reference. (c) Comparison of the Raman spectrum of the bulk and the ball-milled SiNPs at a ∼500 cm^{-1} shift showing a clear shift in the spectrum. (d) Micro-PL spectrum of SiNPs upon excitation with 455 and 532 nm wavelength lasers. PL emission of sapphire substrate was measured and subtracted from the signal of the SiNPs to obtain the presented graphs. Laser artifacts are present in the data marked with blue arrows. Dotted lines represent spectral filters used to cut off excitation laser light.

development and analysis of novel nanomaterials with a complex PL origin, such as SiNPs. The results also suggest that the solvent-free high-energy mechanochemistry is successful in producing visibly emitting SiNPs without the carbon-related nanomaterial fluorescent contaminants.

4. CONCLUSIONS

By combining various microscopic techniques, we show evidence of PL from quantum-confined SiNPs emitting in the visible spectral range. Size-tunable PL emission spectra are observed by AFM-correlated micro-PL spectroscopy. To exclude the role of carbon-related byproducts in the observed PL, we further employ correlative micro-Raman-PL spectroscopy which verifies the PL origin to be from organically capped SiNPs. In this way, we demonstrate a reliable top-down, solvent-free synthesis method with the potential for scale-up for SiNPs with PL in the visible spectral range, which is free of the lately debated fluorescent carbon contaminants. Also, we demonstrate the acute need for correlative microscopy methods in the analysis of the origin of emission from complex nanosized systems. Silicon nanoparticles could be a nontoxic, earth-abundant alternative for light emission applications.

■ ASSOCIATED CONTENT

Supporting Information

The Supporting Information is available free of charge at https://pubs.acs.org/doi/10.1021/acsomega.2c03396.

XPS measurements of the silicon particles, XRD patterns of the unmilled and milled Si particles, DLS results of milled Si nanocrystals, EDX spectrum of the milled Si nanocrystals, and AFM image of 1-octene-capped SiNCs (PDF)

■ AUTHOR INFORMATION

Corresponding Author

Ankit Goyal − *Van der Waals-Zeeman Institute, Institute of Physics, University of Amsterdam, 1098 XH Amsterdam, The Netherlands;* Present Address: Materials Scientist, LeydenJar Technologies BV, Emmy Noetherweg 2D, 2333 BK Leiden, The Netherlands; orcid.org/0000-0002-4076-3980; Email: ankitcct@gmail.com

Authors

Marco van der Laan − *Van der Waals-Zeeman Institute, Institute of Physics, University of Amsterdam, 1098 XH Amsterdam, The Netherlands*

Alessandro Troglia − *Advanced Research Center for Nanolithography, 1098 XG Amsterdam, The Netherlands*

Min Lin − *Department of Biomolecular Nanotechnology, MESA+ Institute, Faculty of Science and Technology, University of Twente, 7500 AE Enschede, The Netherlands*

Harshal Agarwal − *AMOLF, 1098 XG Amsterdam, The Netherlands*

Jorik van de Groep − *Van der Waals-Zeeman Institute, Institute of Physics, University of Amsterdam, 1098 XH Amsterdam, The Netherlands*

Roland Bliem − *Advanced Research Center for Nanolithography, 1098 XG Amsterdam, The Netherlands;* orcid.org/0000-0002-8714-8942

Jos M. J. Paulusse − *Department of Biomolecular Nanotechnology, MESA+ Institute, Faculty of Science and Technology, University of Twente, 7500 AE Enschede, The Netherlands*

Peter Schall − *Van der Waals-Zeeman Institute, Institute of Physics, University of Amsterdam, 1098 XH Amsterdam, The Netherlands;* orcid.org/0000-0003-2612-2762

Katerina Dohnalova − *Van der Waals-Zeeman Institute, Institute of Physics, University of Amsterdam, 1098 XH Amsterdam, The Netherlands;* Present Address: Assistant Professor, Amsterdam University College, Science Park

https://doi.org/10.1021/acsomega.2c03396
ACS Omega 2022, 7, 24881−24887

113, 1098 XG Amsterdam, The Netherlands.; orcid.org/0000-0002-7333-6889

Complete contact information is available at: https://pubs.acs.org/10.1021/acsomega.2c03396

Notes

The authors declare no competing financial interest.

■ ACKNOWLEDGMENTS

We thank D. Giesen, R. Kortekaas, and A. Wattjes for their technical assistance in building the customized ball-mill used in the synthesis of nanoparticles in this study. H.A. acknowledges the Nederlandse Organisatie voor Wetenschappelijk Onderzoek (NWO) VIDI grant (project number 14846).

■ REFERENCES

(1) Wolkin, M. V.; Jorne, J.; Fauchet, M.; Allan, G.; Delerue, C. Electronic States and Luminescence in Porous Silicon Quantum Dots: The Role of Oxygen. *Phys. Rev. Lett.* **1999**, *82*, 197.

(2) Shirahata, N.; Hasegawa, T.; Sakka, Y.; Tsuruoka, T. Size-Tunable UV-Luminescent Silicon Nanocrystals. *Small* **2010**, *6*, 915−921.

(3) https://www.ise.fraunhofer.de/content/dam/ise/de/documents/publications/studies/Photovoltaics-Report.pdf.

(4) Kusova, K. Silicon Nanocrystals: From Indirect to Direct Bandgap. *Phys. Status Solidi A* **2018**, *215*, 1700718.

(5) Kusova, K.; Hapala, P.; Valenta, J.; Jelinek, P.; Cibulka, O.; Ondic, L.; Pelant, I. Direct Bandgap Silicon: Tensile-Strained Silicon Nanocrystals. *Adv. Mater. Interfaces* **2014**, *1*, 1300042.

(6) Dohnalová, K.; Hapala, P.; Kůsová, K.; Infante, I. Electronic Structure Engineering Achieved via Organic Ligands in Silicon Nanocrystals. *Chem. Mater.* **2020**, *32*, 6326−6337.

(7) Dohnalova, K.; Poddubny, A. N; Prokofiev, A. A; de Boer, W. D.; Umesh, C. P; Paulusse, J. M.; Zuilhof, H.; Gregorkiewicz, T. Surface brightens up Si quantum dots: direct bandgap-like size-tunable emission. *Light: Sci. Appl.* **2013**, *2*, No. e47.

(8) Poddubny, A. N.; Dohnalová, K. Direct band gap silicon quantum dots achieved via electronegative capping. *Phys. Rev. B* **2014**, *90*, 245439.

(9) Warner, J. H.; Hoshino, A.; Yamamoto, K.; Tilley, R. D. Water-soluble photoluminescent silicon quantum dots. *Angew. Chem.* **2005**, *117*, 4626−4630.

(10) English, D. S.; Pell, L. S.; Yu, Z.; Barbara, P. F.; Korgel, B. A. Size Tunable Visible Luminescence from Individual Organic Monolayer Stabilized Silicon Nanocrystal Quantum Dots. *Nano Lett.* **2002**, *2*, 681−685.

(11) Wen, X.; Zhang, P.; Smith, T. A.; Anthony, R. J.; Kortshagen, U. R.; Yu, P.; Feng, Y.; Shrestha, S.; Coniber, G.; Huang, S. Tunability Limit of Photoluminescence in Colloidal Silicon Nanocrystals. *Sci. Rep.* **2015**, *5*, 12469.

(12) Mangolini, L.; Jurbergs, D.; Rogojina, E.; Kortshagen, U. Plasma synthesis and liquid-phase surface passivation of brightly luminescent Si nanocrystals. *J. Lumin.* **2006**, *121*, 327−334.

(13) Biesta, W.; van Lagen, B.; Gevaert, V. S.; Marcelis, A. T. M.; Paulusse, J. M. J.; Nielen, M. W. F.; Zuilhof, H. Preparation, Characterization, and Surface Modification of Trifluoroethyl Ester-Terminated Silicon Nanoparticles. *Chem. Mater.* **2012**, *24*, 4311−4318.

(14) Veinot, J. G. C. Synthesis, surface functionalization, and properties of freestanding silicon nanocrystals. *Chem. Commun.* **2006**, 4160−4168.

(15) Wilcoxon, J. P.; Samara, G. A. Tailorable, visible light emission from silicon nanocrystals. *Appl. Phys. Lett.* **1999**, *74*, 3164.

(16) Canham, L. Introductory lecture: origins and applications of efficient visible photoluminescence from silicon-based nanostructures. *Faraday Discuss.* **2020**, *222*, 10−81.

(17) Valenta, J.; Greben, M.; Dyakov, S. A.; Gippius, N. A.; Hiller, D.; Gutsch, S.; Zacharias, M. Nearly perfect near-infrared luminescence efficiency of Si nanocrystals: A comprehensive quantum yield study employing the Purcell effect. *Sci. Rep.* **2019**, *9*, 11214.

(18) Kang, Z.; Liu, Y.; Tsang, C. H. A.; Ma, D. D. D.; Fan, X.; Wong, N. B.; Lee, S. T. Water-Soluble Silicon Quantum Dots with Wavelength-Tunable Photoluminescence. *Adv. Mater.* **2009**, *21*, 661−664.

(19) Warner, J. H.; Rubinsztein-Dunlop, H.; Tilley, R. D. Surface Morphology Dependent Photoluminescence from Colloidal Silicon Nanocrystals. *J. Phys. Chem. B* **2005**, *109*, 19064−19067.

(20) Zhong, Y.; Sun, X.; Wang, S.; Peng, F.; Bao, F.; Su, Y.; Li, Y.; Lee, S. T.; He, Y. Facile, Large-Quantity Synthesis of Stable, Tunable-Color Silicon Nanoparticles and Their Application for Long-Term Cellular Imaging. *ACS Nano* **2015**, *9*, 5958−5967.

(21) Hua, F.; Swihart, M. T.; Ruckenstein, E. Efficient Surface Grafting of Luminescent Silicon Quantum Dots by Photoinitiated Hydrosilylation. *Langmuir* **2005**, *21*, 6054−6062.

(22) Beri, D.; Busko, D.; Mazilkin, A.; Howard, I. A.; Richards, B. S.; Turshatov, A. Highly photoluminescent and stable silicon nanocrystals functionalized via microwave-assisted hydrosilylation. *RSC Adv.* **2018**, *8*, 9979−9984.

(23) Ge, G.; Li, L.; Wang, D.; Chen, M.; Zeng, Z.; Xiong, W.; Wu, X.; Guo, C. Carbon dots: synthesis, properties and biomedical applications. *J. Mater. Chem. B* **2021**, *9*, 6553−6575.

(24) Sharma, V.; Tiwari, P.; Mobin, S. M. Sustainable carbon-dots: recent advances in green carbon dots for sensing and bioimaging. *J. Mater. Chem. B* **2017**, *5*, 8904−8924.

(25) Liu, M. L.; Chen, B. B.; Li, C. M.; Huang, C. Z. Carbon dots: synthesis, formation mechanism, fluorescence origin and sensing applications. *Green Chem.* **2019**, *21*, 449−471.

(26) Wilbrink, J. L.; Huang, C. C.; Dohnalova, K.; Paulusse, J. M. J. Critical assessment of wet-chemical oxidation synthesis of silicon quantum dots. *Faraday Discuss.* **2020**, *222*, 149−165.

(27) Ddungu, J. L. Z.; Silvestrini, S.; Tassoni, A.; De Cola, L. Shedding light on the aqueous synthesis of silicon nanoparticles by reduction of silanes with citrates. *Faraday Discuss.* **2020**, *222*, 350−361.

(28) Matsumoto, T.; Maeda, M.; Kobayashi, H. Photoluminescence Enhancement of Adsorbed Species on Si Nanoparticles. *Nanoscale Res. Lett.* **2016**, *11*, 7.

(29) Wang, L. W.; Zunger, A. Electronic Structure Pseudopotential Calculations of Large (.apprx.1000 Atoms) Si Quantum Dots. *Phys. Chem. A* **1994**, *98*, 2158−2165.

(30) Delerue, C.; Allan, G.; Lannoo, M. Theoretical aspects of the luminescence of porous silicon. *Phys. Rev. B* **1993**, *48*, 11024−11036.

(31) Heintz, A. S.; Fink, M. J.; Mitchell, B. S. Mechanochemical Synthesis of Blue Luminescent Alkyl/Alkenyl-Passivated Silicon Nanoparticles. *Adv. Mater.* **2007**, *19*, 3984−3988.

(32) Goyal, A.; Demmenie, M.; Huang, C. C.; Schall, P.; Dohnalova, K. Photophysical properties of ball milled silicon nanostructures. *Faraday Discuss.* **2020**, *222*, 96.

(33) Goyal, A.; Soni, P. R. Functionally graded nanocrystalline silicon powders by mechanical alloying. *Mater. Lett.* **2018**, *214*, 111−114.

(34) Huang, C. C.; Tang, Y.; van der Laan, M.; van de Groep, J.; Koenderink, A. F.; Dohnalová, K. Band-Gap Tunability in Partially Amorphous Silicon Nanoparticles Using Single-Dot Correlative Microscopy. *ACS Appl. Nano Mater.* **2021**, *4*, 288−296.

(35) Ledoux, G.; Gong, J.; Huisken, F.; Guillois, O.; Reynaud, C. Photoluminescence of size-separated silicon nanocrystals: Confirmation of quantum confinement. *Appl. Phys. Lett.* **2002**, *80*, 4834−4836.

(36) Khoo, K. H.; Zayak, A. T.; Kwak, H.; Chelikowsky, J. R. First-Principles Study of Confinement Effects on the Raman Spectra of Si Nanocrystals. *Phys. Rev. Lett.* **2010**, *105*, 115504.

(37) Gaisler, S. V.; Semenova, O. I.; Sharafutdinov, R. G.; Kolesov, B. A. Analysis of Raman spectra of amorphous-nanocrystalline silicon films. *Phys. Solid State* **2004**, *46*, 1528−1532.

(38) Cleveland, F. F. Raman Spectra of Hydrocarbons I. 1-Octene, cis+trans 2-Octene, trans−3-Octene, trans−4-Octene, 4-Octyne, and 1-Octyne. *J. Chem. Phys.* **1943**, *11*, 1.
(39) Harima, H. Raman scattering characterization on SiC. *Microelectron. Eng.* **2006**, *83*, 126−129.
(40) Fenske, M. R.; Braun, W. G.; Wiegand, R. V.; Quiggle, D.; McCormick, R. H.; Rank, D. H. Raman Spectra of Hydrocarbons. *Anal. Chem.* **1947**, *19*, 700−765.

Recommended by ACS

A Tale of Seemingly "Identical" Silicon Quantum Dot Families: Structural Insight into Silicon Quantum Dot Photoluminescence

Alyxandra N. Thiessen, Jonathan G. C. Veinot, *et al.*

JUNE 29, 2020
CHEMISTRY OF MATERIALS

READ

Silicon Nanocrystals and Their Composites: Syntheses, Fluorescence Mechanisms, and Biological Applications

Jiahao Liang, Xiao Gong, *et al.*

OCTOBER 15, 2019
ACS SUSTAINABLE CHEMISTRY & ENGINEERING

READ

Strain-Induced Spectral Red-Shifting from Nanoscale Frustum Arrays Fabricated over InGaN/GaN Quantum Wells for Light-Emitting Applications

Wai Yuen Fu and Hoi Wai Choi

DECEMBER 29, 2020
ACS APPLIED NANO MATERIALS

READ

Synthesis of Silicates for High-Performance Oxide Semiconductors: Electronic Structure Analysis

Roberto C. Longo, Peter Thissen, *et al.*

NOVEMBER 25, 2020
ACS APPLIED ELECTRONIC MATERIALS

READ

Get More Suggestions >

https://doi.org/10.1021/acsomega.2c03396
ACS Omega 2022, 7, 24881−24887